Original Article

Improved image quality and micronodule detection in thyroid spectral computed tomography using modified swimmer's position

Shuting Liao[1], Nan Zheng[2], Dan Li[2], Chen Liu[2], Haidong Chen[2], Min Cui[3], Xiangrong Yu[2], Chuanmiao Xie[1]

[1]Department of Radiology, Sun Yat-sen University Cancer Center, State Key Laboratory of Oncology in South China, Guangdong Provincial Clinical Research Center for Cancer, Collaborative Innovation Center for Cancer Medicine, Guangdong Key Laboratory of Nasopharyngeal Carcinoma Diagnosis and Therapy, Sun Yat-sen University, Guangzhou, China; [2]Department of Radiology, Zhuhai Hospital Affiliated with Jinan University, Zhuhai People's Hospital, Zhuhai, China; [3]Department of General Surgery, Zhuhai Hospital Affiliated with Jinan University, Zhuhai People's Hospital, Zhuhai, China

Contributions: (I) Conception and design: S Liao, H Chen, X Yu; (II) Administrative support: M Cui, X Yu, C Xie; (III) Provision of study materials or patients: M Cui, X Yu, H Chen; (IV) Collection and assembly of data: S Liao, N Zheng, D Li, C Liu; (V) Data analysis and interpretation: S Liao, N Zheng; (VI) Manuscript writing: All authors; (VII) Final approval of manuscript: All authors.

Correspondence to: Chuanmiao Xie, MD. Department of Radiology, Sun Yat-sen University Cancer Center, State Key Laboratory of Oncology in South China, Guangdong Provincial Clinical Research Center for Cancer, Collaborative Innovation Center for Cancer Medicine, Guangdong Key Laboratory of Nasopharyngeal Carcinoma Diagnosis and Therapy, Sun Yat-sen University, No. 651 Dongfeng Road East, Guangzhou 510060, China. Email: xchuanm@sysucc.org.cn; Xiangrong Yu, MD, PhD. Department of Radiology, Zhuhai Hospital Affiliated with Jinan University, Zhuhai People's Hospital, No. 79 Kangning Road, Zhuhai 519050, China. Email: yuxiangrong@jnu.edu.cn.

Background: Spectral computed tomography (CT) can be used as a valuable complement to ultrasound (US) in the detection of thyroid nodules. This study sought to investigate the effects of various arm positions during thyroid spectral CT scans in terms of radiation exposure, image quality, and micronodule detection (≤10 mm).

Methods: A total of 180 patients (mean age: 48 years; 136 females) who underwent thyroid spectral CT were assigned to the traditional position (TDN; n=60), swimmer's position (SWIM; n=60), and modified swimmer's position (M-SWIM; n=60) groups. Image quality in the plain, arterial, and venous phases was assessed using a 4-point grading scale, the signal-to-noise ratio (SNR), and the contrast-to-noise ratio (CNR). Radiation exposure was assessed using the volume computed tomography dose index ($CTDI_{vol}$), dose-length product (DLP), effective dose of the neck (ED_N), and effective dose of the thyroid (ED_T). The micronodule detection rates for spectral CT and US were compared using the pathology detection rate as a reference.

Results: The M-SWIM group had a significantly higher proportion of 4-point grading, SNR, and CNR than the TDN and SWIM groups (all P<0.001). The $CTDI_{vol}$, DLP, ED_N, and ED_T were similar among the three groups (all P>0.05). The micronodule detection rate was higher in the M-SWIM group than the TDN and SWIM groups (total: 90.6% *vs.* 70.1% *vs.* 46.8%; benign: 89.1% *vs.* 66.7% *vs.* 45.5%; malignant: 94.3% *vs.* 79.5% *vs.* 51.5%; all P<0.001), but comparable to that of the US group (total: 90.6% *vs.* 91.2%; benign: 89.1% *vs.* 90.6%; malignant: 94.3% *vs.* 92.5%; all P>0.05).

Conclusions: The proposed M-SWIM improved the image quality of thyroid spectral CT without increasing the radiation dose, and significantly enhanced the micronodule detection rate.

Keywords: Computed tomography (CT); thyroid; position; radiation dose

Submitted Jun 04, 2024. Accepted for publication Dec 28, 2024. Published online Jan 22, 2025.
doi: 10.21037/qims-24-1119
View this article at: https://dx.doi.org/10.21037/qims-24-1119

Introduction

Ultrasound (US) is the preferred conventional imaging modality for thyroid nodule evaluation (1). However, it has certain limitations, including operator-dependent variability, a limited ability to assess extrathyroidal extension, and difficulties visualizing nodules located in the posterior aspect of the thyroid gland or behind bony structures (2). Computed tomography (CT) addresses these limitations by providing consistent, operator-independent imaging. It also provides multiplanar views of the anatomical location of the thyroid lesion and its relationship with surrounding tissues, as well as a comprehensive visualization of calcifications within the lesion. Recent advances in CT technology such as spectral CT (3) reduce radiation exposure by using dedicated dose-reduced protocols, including noise-reducing reconstruction algorithms, automatic exposure control, raw-data-based filtering techniques, and tube current modulation (4,5). Moreover, spectral CT uses unique post-processing algorithms for artifact correction, and outputs virtual monochromatic images (6) that enhance the inherent anatomical contrast of the thyroid, which in turn improves lesion visualization. Thus, spectral CT can be considered a valuable complement to US.

During routine CT examinations of the thyroid gland, artifacts often appear when the patient is in a traditional position (TDN) (7). This is largely because the thyroid is located at the border of the shoulder and neck, where significant variations in attenuation characteristics are observed. These artifacts significantly affect the visualization of the thyroid and its surrounding structures (8). Adjusting the tube voltage or tube current can slightly reduce these artifacts; however, it also increases the radiation dose. Choi *et al.* (9) leveraged an external traction device to lower the shoulders, resulting in improved image quality for lower cervical spine CT scans. However, this approach requires additional pre-scanning preparations, prolongs the examination time, and relies on patient cooperation. Mueck *et al.* (10) used the swimmer's position (SWIM), where one hand is raised and the other is placed by the side of the body, to reduce image artifacts in cervical spine CT. This approach has improved image quality compared to that of conventional neck CT scans, but artifacts in the thyroid region persist.

In clinical practice, we have observed that image quality could be further improved when using the SWIM for thyroid CT scans, and, importantly, some patients show venous contrast agent retention artifacts during CT scans. Therefore, for the first time, we proposed the modified swimmer's position (M-SWIM), where the lowered hand extends slightly toward the contralateral ilium. This approach not only shifts the relative position of the thyroid in the transverse plane, but also further moves the position of one clavicle forward and the position of the shoulder strap downward in the coronal plane. In addition, the contrast agent is injected into the lowered hand to avoid contrast agent retention.

We hypothesized that the M-SWIM would be a more effective positioning technique that not only enhances the image quality of thyroid CT scans but also improves the detection of thyroid micronodules while minimizing additional radiation exposure. To this end, we compared the effects of three different arm positions (i.e., TDN, SWIM, and M-SWIM) in spectral CT in terms of image quality, radiation exposure, and the detection of thyroid micronodules. We present this article in accordance with the STROBE reporting checklist (available at https://qims.amegroups.com/article/view/10.21037/qims-24-1119/rc).

Methods

Patients

This study was approved by the Institutional Review Board of Zhuhai People's Hospital (No. 202407), and conducted in accordance with the Declaration of Helsinki (as revised in 2013). Written informed consent was obtained from all patients. Patients at Zhuhai People's Hospital who underwent both thyroid US and contrast-enhanced spectral CT examinations, and eventually underwent total thyroidectomy or fine needle aspiration biopsy were enrolled in this study. Clinicians determined the necessity of thyroid CT scans (e.g., to identify whether the nodules had affected the surrounding tissues and lymph nodes). The inclusion and exclusion criteria are detailed in the Supplementary file (Appendix 1).

Spectral CT protocol

All thyroid CT scans were performed using a 256-detector row CT scanner (New Revolution CT, GE Healthcare, USA) under the Gemstone Spectral Imaging mode. The patients were instructed on how to position their bodies, and advised not to swallow during the scan to keep the neck relatively still. The scan was performed from head to toe, from the base of the skull to the level of the third thoracic vertebra. The following parameters were used: rapid tube

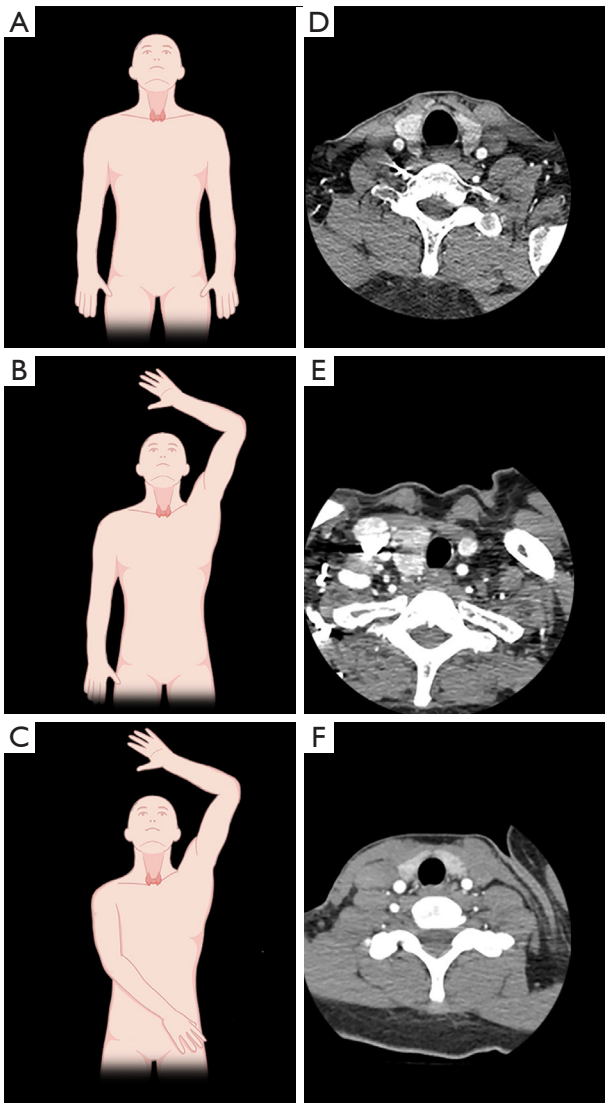

Figure 1 Arm positions, thyroid CT images, as well as regions of interest plotting. (A) Patients in the TDN group were positioned traditionally, with their hands on both sides of the body. (B) Patients in the SWIM group were positioned in the swimmer's position, with one arm positioned above the head and the other arm lateral to the body. (C) Patients in the M-SWIM group were positioned in an improved SWIM, with one arm positioned above the head, and the other arm lateral to the body, and stretched to the contralateral ilium. (D) The arterial phase CT image of the thyroid using TDN was scored 2 for the objective evaluation due to the beam artifact. (E) The arterial phase CT image of the thyroid using SWIM was scored 2 due to the contrast artifact. (F) The arterial phase CT image of the thyroid using M-SWIM was scored 4, as it had no artifacts. CT, computed tomography; TDN, traditional position; SWIM, swimmer's position; M-SWIM, modified swimmer's position.

voltage: fast switching between 80 and 140 kVp (0.5 ms); tube current: 50% adaptive statistical iterative reconstruction with a noise index of 5.5; rotation time: 0.5 s/rotation; pitch: 0.992:1; collimation width: 64×0.625 mm; slice thickness: 1.25 mm; slice interval: 1 mm; and reconstruction matrix: 512×512. Prior to the contrast-enhanced scan, all patients received a nonionic contrast agent, iohexol (320 mg I/mL), which was injected at a rate of 3 mL/s (dose: 1.5–2 mL/kg). The plain phase was performed before enhanced scanning rather than non-virtual contrast image, as the latter relies on algorithms and may result in unstable image quality. The arterial phase scan was performed 25 seconds after contrast injection, followed by a delayed 25-second scan for the venous phase images. To ensure overall image quality (11), all images were transferred to a workstation (AW version 4.6, GE Healthcare, USA) to generate images at 70 keV as the output for monoenergetic imaging.

The scan positions were as follows: TDN: supine position with arms naturally hanging down at the sides; SWIM: supine position with one arm raised, and the other arm naturally hanging down at the side; and M-SWIM: supine position with one arm raised, and the other arm hanging down and extended to the opposite iliac bone. In the SWIM and M-SWIM, the left arm was fixed in the raised position, and the injection arm was the right arm. The scanning technicians instructed each patient on the positioning. Illustrations of the three arm positions are provided in *Figure 1*.

Image quality evaluation and radiation dose calculation

Image quality evaluation

Two experienced radiologists (with 10 years of experience each in head and neck imaging) read the images on the optimal reconstruction field of view (rather than the shoulder girdle or scout views). Using a 4-point image grading scale, on which 1 represented severe artifacts, 2 represented moderate artifacts, 3 represented mild artifacts, and 4 represented no artifacts, the two readers independently evaluated the images of the three groups. For further details on the 4-point image grading scale, see the Supplementary file (Appendix 1). In cases of disagreement, consensus was reached through discussion.

The four regions of interest (ROIs) were the thyroid gland (ROI_T), muscles surrounding the thyroid gland (ROI_M), posterior neck muscles (ROI_{PM}), and internal jugular vein (ROI_V) at the level of the 7th cervical vertebra to the 2nd thoracic vertebra (*Figure 2*). Notably, the ROI_T

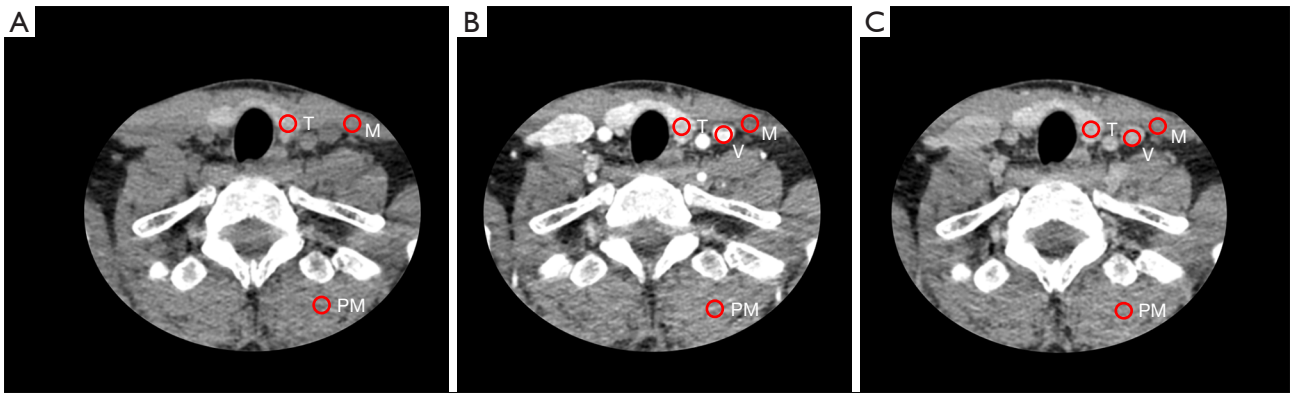

Figure 2 Illustration of the delineation of the ROIs. (A) In the plain phase, three ROIs consisting of ROI_T, ROI_M, and ROI_{PM} were separately placed on the thyroid gland, muscles surrounding the thyroid gland, and posterior neck muscles at the level of the 7th cervical vertebra to the 2nd thoracic vertebra. (B) In the arterial phase, the ROI_T, ROI_M, ROI_{PM}, and ROI_V were placed on the thyroid gland, muscles surrounding the thyroid gland, posterior neck muscles, and internal jugular vein at the same level. (C) In the venous phase, the ROI_T, ROI_M, ROI_{PM}, and ROI_V were placed on the thyroid gland, muscles surrounding the thyroid gland, posterior neck muscles, and internal jugular vein at the same level. The red circles represent each ROI with a standard 0.3–0.5 cm^2 square area, and were used to measure the CT values in HUs and their SDs to calculate the SNR and CNR. ROIs, regions of interest; ROI_T, thyroid gland region of interest; ROI_M, muscles surrounding the thyroid gland region of interest; ROI_{PM}, posterior neck muscles region of interest; ROI_V, internal jugular vein region of interest; HUs, Hounsfield units; SDs, standard deviations; SNR, signal-to-noise ratio; CNR, contrast-to-noise ratio.

excluded areas of cystic degeneration and calcification. The CT values [Hounsfield units (HU)] and image noise values [standard deviation (SD)] were measured from the ROIs. The signal-to-noise ratio (SNR) and contrast-to-noise ratio (CNR) were calculated to assess image quality (12). The SD value of the posterior neck muscle without artifacts at the same level was used as the background noise. If the CNR value was negative, its absolute value was adopted. The equations for SNR and CNR are expressed as follows:

$$SNR_T = CT\ value\ of\ ROI_T / SD\ of\ ROI_{PM} \quad [1]$$

$$SNR_M = CT\ value\ of\ ROI_M / SD\ of\ ROI_{PM} \quad [2]$$

$$SNR_V = CT\ value\ of\ ROI_V / SD\ of\ ROI_{PM} \quad [3]$$

$$CNR_{T\text{-}M} = SNR_T - SNR_M \quad [4]$$

$$CNR_{T\text{-}V} = SNR_T - SNR_V \quad [5]$$

Calculation of radiation dose

The volume computed tomography dose index ($CTDI_{vol}$) and dose-length product (DLP) (13) of the three groups were documented in the picture archiving and communication system. The effective dose of the neck (ED_N) and the effective dose of the thyroid (ED_T) were calculated using the formula DLP × W, where W is the conversion factor based on the International Commission on Radiological Protection coefficients. The conversion factors used were W_N (conversion factor for neck effective dose): 0.0059 mSv/mGy × cm, and W_T (conversion factor for thyroid effective dose): 0.04 mSv/mGy × cm (14,15). The data for ED_N and ED_T were recorded separately, and the mean and SD were calculated.

To examine the effects of the body mass index (BMI) and effective diameter of the neck (EDN) on the radiation dose, the two confounders were compared among the three groups. The EDN was measured on an axial CT image at the level of the upper margin of the tracheal cartilage (5).

Comparison of the micronodule detection rates

Two senior radiologists independently reviewed the thyroid spectral CT images with the three arm positions to identify micronodules (≤10 mm) from all nodules. The US images and reports were also screened by two sonographers. In cases of disagreement, consensus was reached by discussion. The ability of spectral CT and US to detect benign and malignant micronodules was then compared using the postsurgical pathology results as a reference. The post-operative pathology results included the number, location, and size of the nodules in the resected thyroid tissue, as well

Table 1 Patient characteristics

Variables	TDN group (N=60)	SWIM group (N=60)	M-SWIM group (N=60)	P value
Age (years)	48±12	50±13	46±12	0.212
Gender				0.396
Male	17 (28.0)	16 (27.0)	11 (18.0)	
Female	43 (72.0)	44 (73.0)	49 (82.0)	
BMI (kg/m^2)	23.8±3.1	24.3±3.8	23.6±3.2	0.449
EDN (cm)	12.8±1.2	13.0±1.5	13.0±1.6	0.629
Micronodule				0.225
Benign	123 (78.8)	120 (73.2)	128 (70.7)	
Malignant	33 (21.2)	44 (26.8)	53 (29.3)	

Continuous variables are expressed as the mean ± standard deviation, while the categorical and ordinal data are presented as the n (%). BMI, body mass index; EDN, effective diameter of the neck; TDN, traditional position; SWIM, swimmer's position; M-SWIM, modified swimmer's position.

as the benign or malignant nature of the nodules.

Statistical analysis

The Kruskal-Wallis *H* test was used to compare the categorical variables, while an analysis of variance was used to compare the continuous variables. If a significant difference was found, a post-hoc Student-Newman-Keuls test was used for multiple comparisons, unless otherwise stated. The Chi-square test was used to compare the detection rates among the three groups. All the statistical analyses were performed using SPSS (version 22.0, Armonk, NY, USA). A P value <0.05 was considered statistically significant.

Results

Patient characteristics

The patient characteristics are shown in *Table 1*. The average age of the patients was 48 years, and 136 (75.6%) of the patients females. The malignancy rates were 21.2% (33/156), 26.8% (44/164), and 29.3% (53/181) in the TDN, SWIM, and M-SWIM groups, respectively. No significant differences were observed among the three groups in terms of age, sex, BMI, EDN, and malignant prevalence (all P>0.05).

Comparison of image quality and radiation dose

Image quality

As *Figure 3* shows, the M-SWIM group had the highest score across all three scanning phases [plain phase: 46.7% (28/60); arterial phase: 66.7% (40/60); venous phase: 63.3% (38/60)], followed by the SWIM group [plain phase: 31.7% (19/60); arterial phase: 46.7% (28/60); venous phase: 41.7% (25/60)], and the TDN group [plain phase: 13.3% (8/60); arterial phase: 20.0% (12/60); venous phase: 16.7% (10/60)]. Notably, no patients in the SWIM and M-SWIM groups received a grading score of one, but this did occur in the TDN group in the subjective assessment of image quality. Accordingly, the M-SWIM group had higher image quality than the SWIM and TDN groups (all P<0.001).

The SNR and CNR were used for the objective assessment of image quality. As *Table 2* shows, compared to the SWIM and TDN groups, the M-SWIM group had superior image quality across all three scanning phases (all P<0.001). In the plain phase, the average SNR and CNR were much higher in the M-SWIM group than in the SWIM and TDN groups (SNR_T: 11.8 *vs.* 8.7 *vs.* 5.9; SNR_M: 7.8 *vs.* 5.5 *vs.* 4.6; CNR_{T-M}: 4.0 *vs.* 3.2 *vs.* 2.6, all P<0.001). A similar trend was observed in the arterial and venous phases; the M-SWIM group also had the highest mean SNR and CNR compared to the SWIM and TDN groups (arterial phase, SNR_T: 19.2 *vs.* 14.8 *vs.* 9.8, SNR_M: 7.8 *vs.* 5.5 *vs.* 3.5, CNR_{T-M}: 11.4 *vs.* 9.2 *vs.* 6.3, SNR_V: 19.2 *vs.* 12.1 *vs.* 9.2, CNR_{T-V}: 5.0 *vs.* 4.0 *vs.* 2.5; venous phase, SNR_T: 18.1 *vs.* 13.2 *vs.* 8.8, SNR_M: 8.5 *vs.* 5.6 *vs.* 4.0, CNR_{T-M}: 9.6 *vs.* 7.5 *vs.* 4.7, SNR_V: 19.2 *vs.* 11.9 *vs.* 9.3, CNR_{T-V}: 3.8 *vs.* 2.6 *vs.* 1.5, all P<0.001). Collectively, the M-SWIM group had better image quality than the other two groups.

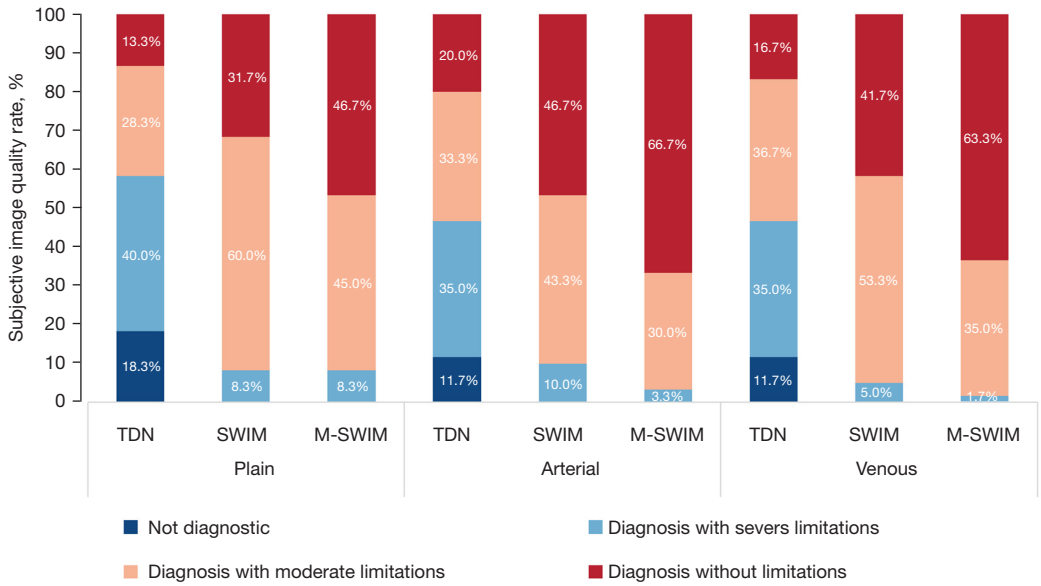

Figure 3 A stacked column chart displays the subjective evaluation results for the image quality of the TDN, SWIM, and M-SWIM groups in the three scanning phases. TDN, traditional position; SWIM, swimmer's position; M-SWIM, modified swimmer's position.

Table 2 Comparison of objective assessment image quality among the TDN, SWIM, and M-SWIM groups

Image quality indicators	Phase	TDN group (n=60)	SWIM group (n=60)	M-SWIM group (n=60)	P value
SNR_T	Plain	5.9±2.9	8.7±2.3	11.8±3.2	<0.001
	Arterial	9.8±4.0	14.8±5.9	19.2±6.0	<0.001
	Venous	8.8±3.4	13.2±5.0	18.1±4.5	<0.001
SNR_M	Plain	4.6±2.0	5.5±1.4	7.8±1.9	<0.001
	Arterial	3.5±1.5	5.5±2.0	7.8±1.7	<0.001
	Venous	4.0±1.4	5.6±2.0	8.5±1.8	<0.001
CNR_{T-M}	Plain	2.6±1.8	3.2±1.4	4.0±1.9	<0.001
	Arterial	6.3±3.1	9.2±4.4	11.4±4.7	<0.001
	Venous	4.7±2.6	7.5±3.3	9.6±3.1	<0.001
SNR_V	Arterial	9.2±5.2	12.1±6.7	19.2±9.0	<0.001
	Venous	9.3±3.7	11.9±4.4	19.2±5.8	<0.001
CNR_{T-V}	Arterial	2.5±2.2	4.0±2.6	5.0±3.1	<0.001
	Venous	1.5±1.2	2.6±2.2	3.8±2.4	<0.001

Continuous variables are expressed as the mean ± standard deviation. SNR_M was defined as the ratio of the CT value of the soft tissue surrounding the thyroid gland to the background noise at the C7 to T2 level; SNR_T was defined as the ratio of the CT value of the thyroid to the background noise at the C7 to T2 level; CNR_{T-M} was defined as the difference between SNR_T and SNR_M, which is the contrast index between the thyroid gland and its surrounding muscle tissue; SNR_V was defined as the ratio of the CT value of the internal jugular vein to the background noise at the C7 to T2 level; CNR_{T-V} was defined as the difference between SNR_T and SNR_V; that is, the contrast index between the thyroid gland and its adjacent enhanced internal jugular vein. TDN, traditional position; SWIM, swimmer's position; M-SWIM, modified swimmer's position; SNR, signal-to-noise ratio; CNR, contrast-to-noise ratio.

Table 3 Comparison of radiation exposure of TDN, SWIM, and M-SWIM groups

Radiation exposure	Phase	TDN group (n=60)	SWIM group (n=60)	M-SWIM group (n=60)	P value
$CTDI_{vol}$ (mGy)	Plain	18.8±1.2	18.2±1.8	18.1±1.7	0.095
	Arterial	18.2±1.9	17.5±2.4	17.1±2.5	0.055
	Venous	18.2±1.9	17.5±2.4	17.1±2.5	0.055
DLP (mGy·cm)	Plain	405.2±50.2	394.5±62.0	392.3±62.3	0.056
	Arterial	390.6±62.3	368.9±66.8	363.1±67.7	0.052
	Venous	389.5±62.3	369.0±66.8	363.1±67.7	0.052
ED_N (mSv)	Total	7.0±1.0	6.7±1.1	6.6±1.1	0.109
ED_T (mSv)	Total	47.4±6.6	45.3±7.6	44.7±7.6	0.109

Continuous variables are expressed as mean ± standard deviation. TDN, traditional position; SWIM, swimmer's position; M-SWIM, modified swimmer's position; $CTDI_{vol}$, volume computed tomography dose index; DLP, dose-length product; ED_N, effective dose of the neck; ED_T, effective dose of the thyroid.

Radiation dose

Table 3 shows the radiation dose of thyroid spectral CT using TDN, SWIM, and M-SWIM. Overall, there were no significant differences in the radiation exposure metrics, including the $CTDI_{vol}$, DLP, ED_N, and ED_T, among the three groups (all P>0.05). Compared with the TDN group, the ED_N and ED_T of the M-SWIM group were reduced by 5.7% (6.6±1.1 *vs.* 7.0±1.0 mGy, P=0.109) and 5.7% (44.7±7.6 *vs.* 47.4±6.6 mGy, P=0.109), respectively. The post-hoc analysis showed that the radiation doses between the SWIM and M-SWIM groups was similar but were lower than that of the TDN group. The results suggested that the M-SWIM did not increase the radiation dose.

Comparison of the micronodule detection rates

Figure 4 shows the thyroid micronodule detection rates using spectral CT and US. For US, the detection rates of the total [90.4% (141/156) *vs.* 90.9% (149/164) *vs.* 91.2% (165/181), P=0.970], benign [91.1% (112/123) *vs.* 90.8% (109/120) *vs.* 90.6% (116/128), P=0.993], and malignant [87.9% (29/33) *vs.* 90.9% (40/44) *vs.* 92.5% (49/53), P=0.775] micronodules in the TDN, SWIM, and M-SWIM groups did not differ significantly (all P>0.05). However, the detection rates of the TDN, SWIM, and M-SWIM groups varied, such that the M-SWIM group had the highest detection rate followed by the SWIM group and the TDN group [total: 90.6% (164/181) *vs.* 70.1% (115/164) *vs.* 46.8% (73/156), P<0.001; benign: 89.1% (114/128) *vs.* 66.7% (80/120) *vs.* 45.5% (56/123), P<0.001; malignant: 94.3% (50/53) *vs.* 79.5% (35/44) *vs.* 51.5% (17/33), P<0.001].

Additionally, the micronodule detection rates were compared between spectral CT and US; in the TDN group, statistically significant differences were found in the total, benign, and malignant micronodule detection rates (all P<0.001); in the SWIM group, significant differences were found in the total and benign micronodule detection rates (both P<0.001), but no statistically significant difference was found in the malignant micronodule detection rate (P=0.133); and in the M-SWIM group, no significant differences were found in the total (P=0.855), benign (P=0.696), and malignant (P=0.679) micronodule detection rates.

Discussion

Previous studies (9,16) used a table cloth and an external device to manipulate the shoulder position downward, and reported that this maneuver reduces the artifacts (17) caused by significant attenuation changes in lower neck CT scans due to variations in body thickness. Other studies (10,18) have explored the SWIM and found that adjusting the patient's arm position can address this issue. However, in our use of the SWIM in clinical practice, we observed that image quality could be further improved.

Most studies (9,16,19) have primarily focused on the image quality of the lower cervical spine, neglecting that of the thyroid gland in the anterior neck. The improvement in body thickness scanning was limited to the axial position, and contrast media residue in the subclavian vein posed a potential obstacle to optimizing the SWIM for thyroid

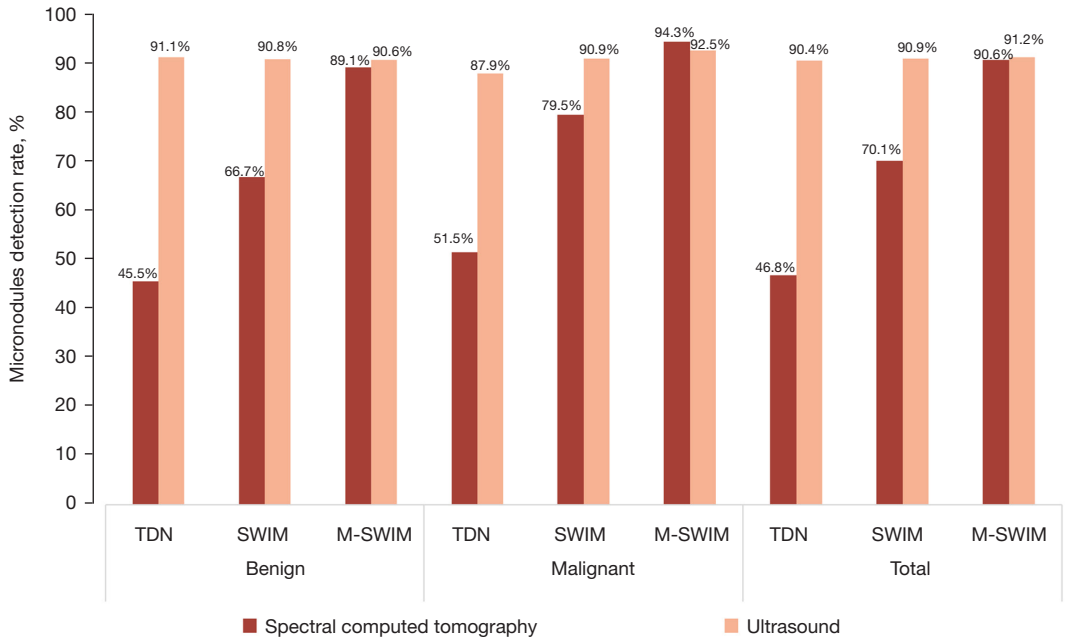

Figure 4 Detection rates of micronodules using ultrasound and spectral computed tomography based on TDN, SWIM, and M-SWIM. TDN, traditional position; SWIM, swimmer's position; M-SWIM, modified swimmer's position.

scanning. Consequently, we proposed the M-SWIM, which involves injecting contrast media into the lower hand, and extending it obliquely toward the contralateral ilium. The M-SWIM enhances the relative anatomical alignment of the bilateral clavicles, shoulders, and thyroid gland in both the axial and coronal planes, thereby enabling the clearer visualization of the thyroid gland in CT images. Additionally, while the previous generation of CT machines lacked advanced capabilities, our study leveraged spectral CT with rapid scanning technology and adaptive statistical iterative reconstruction for thyroid gland imaging (20). Further, the application of the Revolution GE CT spectral imaging mode with an automatic anti-artifact algorithm and monochromatic image acquisition facilitated the generation of low-noise thyroid images, enabling the more effective analysis of thyroid nodules (21). Previous studies (10,22) using the SWIM have also reported that optimizing shoulder position and hand placement to reduce body thickness in the lower neck can minimize radiation exposure during scanning. Therefore, by using advanced CT machines, such as spectral CT, the M-SWIM can effectively mitigate beam artifacts in thyroid CT images without subjecting the patient to additional radiation exposure.

Using M-SWIM, the artifacts in the thyroid CT images were significantly reduced, as was the level of image noise. In the subjective evaluation, 12 (20.0%) patients in the TDN group, 28 (46.7%) patients in the SWIM group, and 40 (66.7%) patients had the highest scores. Instead of only measuring the attenuation values and SDs of the ROIs placed on the thyroid and surrounding structures, we calculated the SNR and CNR to assess the image quality. The SNR quantifies image quality by comparing the objective noise to the background noise (23). The CNR indicates the relative image quality and visibility of the target lesion. From a lesion visibility perspective, only the CNR needs to be increased, and increasing contrast is equivalent to reducing noise (24). Therefore, the SNR and CNR intuitively describe the noise and contrast between the thyroid and the surrounding structures. The results showed that compared to the TDN and SWIM groups, the SNR and CNR were improved in the M-SWIM group, especially during the arterial phase. This is because images acquired in the arterial phase not only have beam artifacts like the other phases but also have artifacts caused by contrast media remaining in the subclavian vein, which are effectively reduced by M-SWIM.

To reduce the beam and contrast media artifacts, we adjusted the shoulder girdle angle to >10° and positioned the arm in which the contrast medium was injected low and extended to the opposite ilium. In our study, the M-SWIM

served this purpose well, but it has been rarely discussed in previous literature. To easily improve image quality, the effect of increasing the tube voltage or tube current is obvious, but this also increases the radiation dose. However, attempts should be made to maintain low radiation doses to avoid increasing the risk of tumors caused by the stochastic effects of CT radiation exposure (25), and because the thyroid gland is a radiation-sensitive organ. Compared to the TDN group, the radiation exposure metrics, such as the ED_N and ED_T, showed a tendency to decrease in the SWIM and M-SWIM groups. It might be that the optimal shoulder position resulted in a decreased bone and soft tissue volume within the constant scanning range. This would increase the likelihood of keeping the image noise constant, and reaching the maximum tube current during scanning with automated tube current modulation. Thus, our current results suggest that using a simple arm positioning strategy like M-SWIM in routine practice with cooperative patients could easily improve thyroid CT image quality without any additional radiation exposure, financial costs related to extra devices, or discomfort to the patient.

We also explored the efficacy of detecting thyroid micronodules to aid in the early identification of potential malignancies, reduce the risk of tumor progression, and raise health awareness among patients. After comparing the CT and US micronodule detection rates, significant differences were observed in the TDN group. In the SWIM group, there were statistically significant differences in the detection rates of total and benign micronodules between CT and US, but no such difference was observed in relation to the malignant micronodules. The M-SWIM group had a malignant micronodule detection rate of 94.3%, which was slightly higher than the US detection rate of 92.5%. Further, the total and benign micronodule detection rates were 90.6% and 89.1%, respectively, which were close to the US detection rates (total: 91.2%, benign: 90.6%). Additionally, the CT total micronodule detection rate of the M-SWIM group was 20.5% higher than that of the SWIM group, and 43.8% higher than that of the TDN group. These findings suggest that the application of M-SWIM for thyroid CT scanning significantly improved micronodule detection compared to US, and M-SWIM also improved thyroid CT image quality. Clear thyroid CT images obtained in the M-SWIM position can complement those obtained by US, as they better show microcalcifications and their dense distribution patterns, and can be used to evaluate deep-seated nodules, and enable detailed multiplanar assessments. Additionally, spectral CT provides further valuable measurements of functional iodine uptake, aiding in the differentiation of benign and malignant nodules. Clearer CT images could serve as an indispensable complementary tool to optimize clinical decision making.

This study had some limitations. First, the clinical applicability of the arm positioning strategy was limited to patients who were cooperative and did not have any physical disabilities in their arms. Second, while efforts were made to balance the BMI, EDN, and scan lengths, these differed in the patients. The use of identical subjects in all three groups and the use of the same scanning parameters would have provided a more accurate assessment of the exact effect of the arm positioning strategies on CT image quality and radiation dose. However, it is ethically challenging to collect data from the same subjects in a clinical setting. Therefore, in the future, phantom studies or well-designed prospective studies should be conducted to validate the current findings.

Conclusions

Our findings showed that the M-SWIM was more effective than the TDN and SWIM in reducing imaging artifacts, and also improved the detection of micronodules in thyroid spectral CT. Moreover, patients undergoing thyroid CT in the M-SWIM did not experience any additional radiation exposure compared to those in the TDN and SWIM.

Acknowledgments

None.

Footnote

Reporting Checklist: The authors have completed the STROBE reporting checklist. Available at https://qims.amegroups.com/article/view/10.21037/qims-24-1119/rc

Funding: This work was supported by the National Natural Science Foundation of China (No. 82071915 to X.Y.), and Guangdong Basic and Applied Basic Research Foundation (No. 2022A1515220015 to X.Y.).

Conflicts of Interest: All authors have completed the ICMJE uniform disclosure form (available at https://qims.amegroups.com/article/view/10.21037/qims-24-1119/coif). X.Y. reports that this work received funding from the National Natural Science Foundation of China (No. 82071915), and Guangdong Basic and Applied Basic

Research Foundation (No. 2022A1515220015). The other authors have no conflicts of interest to declare.

Ethical Statement: The authors are accountable for all aspects of the work in ensuring that questions related to the accuracy or integrity of any part of the work are appropriately investigated and resolved. The study was conducted in accordance with the Declaration of Helsinki (as revised in 2013). The study was approved by Institutional Review Board of Zhuhai People's Hospital (approval No. 202407), and informed consent was obtained from all patients.

References

1. Ha EJ, Baek JH, Na DG. Risk Stratification of Thyroid Nodules on Ultrasonography: Current Status and Perspectives. Thyroid 2017;27:1463-8.
2. Haugen BR. 2015 American Thyroid Association Management Guidelines for Adult Patients with Thyroid Nodules and Differentiated Thyroid Cancer: What is new and what has changed? Cancer 2017;123:372-81.
3. Zhao YX, Suo HN, Zuo ZW, Xu YJ, Chang J. A Comparison of the Image Quality and Radiation Dose With Routine Computed Tomography and the Latest Gemstone Spectral Imaging Combination of Different Scanning Protocols in Computed Tomography Angiography of the Kidney. J Comput Assist Tomogr 2017;41:263-70.
4. Deak PD, Smal Y, Kalender WA. Multisection CT protocols: sex- and age-specific conversion factors used to determine effective dose from dose-length product. Radiology 2010;257:158-66.
5. Bankier AA, Kressel HY. Through the Looking Glass revisited: the need for more meaning and less drama in the reporting of dose and dose reduction in CT. Radiology 2012;265:4-8.
6. Albrecht MH, Vogl TJ, Martin SS, Nance JW, Duguay TM, Wichmann JL, De Cecco CN, Varga-Szemes A, van Assen M, Tesche C, Schoepf UJ. Review of Clinical Applications for Virtual Monoenergetic Dual-Energy CT. Radiology 2019;293:260-71.
7. Barrett JF, Keat N. Artifacts in CT: recognition and avoidance. Radiographics 2004;24:1679-91.
8. Jiang L, Liu D, Long L, Chen J, Lan X, Zhang J. Dual-source dual-energy computed tomography-derived quantitative parameters combined with machine learning for the differential diagnosis of benign and malignant thyroid nodules. Quant Imaging Med Surg 2022;12:967-78.
9. Choi YJ, Lee JH, Cho WY, Baek JH. Effect of an arm traction device on image quality and radiation exposure during neck computed tomography. Eur J Radiol 2016;85:68-72.
10. Mueck FG, Roesch S, Geyer L, Scherr M, Seidenbusch M, Stahl R, Deak Z, Wirth S. Emergency CT head and neck imaging: effects of swimmer's position on dose and image quality. Eur Radiol 2014;24:969-79.
11. Jacobsen MC, Schellingerhout D, Wood CA, Tamm EP, Godoy MC, Sun J, Cody DD. Intermanufacturer Comparison of Dual-Energy CT Iodine Quantification and Monochromatic Attenuation: A Phantom Study. Radiology 2018;287:224-34.
12. Eck BL, Fahmi R, Brown KM, Zabic S, Raihani N, Miao J, Wilson DL. Computational and human observer image quality evaluation of low dose, knowledge-based CT iterative reconstruction. Med Phys 2015;42:6098-111.
13. Inoue Y, Itoh H, Waga A, Sasa R, Mitsui K. Radiation Dose Management in Pediatric Brain CT According to Age and Weight as Continuous Variables. Tomography 2022;8:985-98.
14. Boone JM, Brink JA, Edyvean S, Huda W, Leitz W, McCollough CH, McNitt-Gray MF. 4. Overview of Existing CT-Dosimetry Methods. Journal of the ICRU 2012;12:35-45.
15. Andersson M, Johansson L, Minarik D, Leide-Svegborn S, Mattsson S. Effective dose to adult patients from 338 radiopharmaceuticals estimated using ICRP biokinetic data, ICRP/ICRU computational reference phantoms and ICRP 2007 tissue weighting factors. EJNMMI Phys 2014;1:9.
16. Kranz PG, Wylie JD, Hoang JK, Kosinski AS. Effect of the CT table strap on radiation exposure and image quality during cervical spine CT. AJNR Am J Neuroradiol 2014;35:1870-6.
17. Marshall EL, Ginat DT, Sammet S. Computed Tomography Imaging Artifacts in the Head and Neck Region: Pitfalls and Solutions. Neuroimaging Clin N Am

2022;32:271-7.
18. Kane AG, Reilly KC, Murphy TF. Swimmer's CT: improved imaging of the lower neck and thoracic inlet. AJNR Am J Neuroradiol 2004;25:859-62.
19. Zhang L, Zhao B, Wang S, Wang Y, Yan Y, Tian X. Optimisation of monoenergetic images to reduce banding artifacts in the lower cervical spine using dual-layer spectral computed tomography: a retrospective study. Clin Radiol 2024;79:e1252-9.
20. Liu Z, Zhang Z, Chen C, Hong N. Value of virtual monochromatic spectral images with metal artifact reduction algorithm in dual-energy computed tomography-guided microcoil localization of pulmonary nodules. Medicine (Baltimore) 2018;97:e11562.
21. Fang T, Deng W, Law MW, Luo L, Zheng L, Guo Y, Chen H, Huang B. Comparison of image quality and radiation exposure between conventional imaging and gemstone spectral imaging in abdominal CT examination. Br J Radiol 2018;91:20170448.
22. Wirth S, Meindl T, Treitl M, Pfeifer KJ, Reiser M. Comparison of different patient positioning strategies to minimize shoulder girdle artifacts in head and neck CT. Eur Radiol 2006;16:1757-62.
23. Boedeker KL, McNitt-Gray MF. Application of the noise power spectrum in modern diagnostic MDCT: part II. Noise power spectra and signal to noise. Phys Med Biol 2007;52:4047-61.
24. Huda W, Abrahams RB. Radiographic techniques, contrast, and noise in x-ray imaging. AJR Am J Roentgenol 2015;204:W126-31.
25. Almohiy H. Paediatric computed tomography radiation dose: A review of the global dilemma. World J Radiol 2014;6:1-6.

Cite this article as: Liao S, Zheng N, Li D, Liu C, Chen H, Cui M, Yu X, Xie C. Improved image quality and micronodule detection in thyroid spectral computed tomography using modified swimmer's position. Quant Imaging Med Surg 2025;15(2):1571-1581. doi: 10.21037/qims-24-1119

